A New Silicone Structure for uSkin - a Soft, Distributed, Digital 3-axis Skin Sensor - and its Integration on the Humanoid Robot iCub

Tito Pradhono Tomo[1], Massimo Regoli[2], Alexander Schmitz[1], Lorenzo Natale[2],
Harris Kristanto[1], Sophon Somlor[1], Lorenzo Jamone[3], Giorgio Metta[2] and Shigeki Sugano[1]

Abstract—Tactile sensing is one important element that can enable robots to interact with an unstructured world. By having tactile perception, a robot can explore its environment by touching objects. Like human skin, a tactile sensor that can provide rich information such as distributed normal and shear forces with high density can help the robot to recognize objects. In previous work we introduced uSkin, a soft skin with distributed 3-axis force sensitive elements, and a center-to-center distance between the 3-axis load cells of 4.7 mm for the flat version. The current paper presents a new structure for the distributed soft force transducer which reduces the crosstalk between the components of the 3-axis force measurements. 3D printing the silicone structure eased the prototype production. However, the 3D printed material has a higher hysteresis than the previously used Ecoflex. Microcontroller boards originally developed for the skin of iCub were implemented for uSkin, increasing the readout frequency and reducing the space requirements and number of wires. The sensor was installed on iCub and successfully used for shape exploration.

Index Terms—Force and Tactile Sensing, Dexterous Manipulation, Multifingered Hands.

I. INTRODUCTION

TO interact with challenging dynamic environments, it is crucial for robots to have an ability to sense what they are touching or of being touched. Covering robots with tactile sensors is one way to give them a touch perception so that they can learn to perform stable, subtle, and precise object manipulation. Moreover, robots can also recognize an object shape or location by performing tactile exploration. Distributed skin sensors can provide richer information than sensors in the robot joints [1]. To give more accurate information, it is important that the skin sensors have a rather high spatial density and measure 3-axis force. However, a 3D sensor with high spatial density usually introduces problems such as large number of wires and bulky electronics (amplifier, analog to digital converter, etc.).

Furthermore, adaptability is important so that the skin sensors can be used for various robot platforms, i.e. it should be possible to adjust the sensor to various requirements. For example, contact materials with high surface friction such as silicone are preferable for stable grasping while for social robots that are more engaged in human-robot interaction materials with less friction such as fabric are preferable, as high friction could lead to painful situations. Fabric is also better for sliding the sensor across surfaces, somewhat more robust (partially due to the reduced friction), and can be used as an interchangeable surface layer, making repairs easier. The skin should also be light and able to cover large areas [2] [3] [4]. Developing a skin sensor that can be adapted for various robot applications and at the same time can measure normal and shear forces with a high spatial density, requiring minimal wiring and electronics and able to cover most robot parts is a huge challenge in the robotics field.

We have been working on developing a skin sensor that can meet all of these requirements [5] [6] [7]. We named our skin sensor "uSkin". uSkin in this paper is based on the one introduced in [6], in particular the current paper uses a nearly identical PCB (printed circuit board) with 16 3-axis Hall effect sensors. The center-to-center distance between the 3-axis sensors is 4.7 mm. In our previous work the skin was manufactured by simply embedding permanent magnets inside bulk silicone rubber (without any cavity or particular structure). As silicone is incompressible, the permanent magnets also displaced sideways when force was applied perpendicular to the surface of the skin. This causes severe crosstalk between the 3 measurement axes and makes a calibration procedure necessary. Calibrating the sensors is a time consuming process, especially for a distributed sensor with many measurements. We assume that decoupling the measurement axes will result in no more need to calibrate the sensors for certain applications (where the direction is more important than the force value, e.g. in a joystick like user interface). If calibrated force readings are required, the calibration procedure could be easier, requiring less calibration parameters and therefore less calibration data (by ignoring the crosstalk between the measurement axes), even more so when combined with a linear (instead of quadratic) calibration model. For this reason, in this paper we will introduce uSkin with an improved soft skin structure. Furthermore, structured silicone with air gaps can reduce the crosstalk between neighboring 3-axis measurements, can be softer, and have less hysteresis than

bulk silicone, but this also depends on the used materials, and is not fully explored in this paper.

In [6] and [7], we integrated uSkin into an Allegro hand. However, uSkin can also be used to cover other robots. To demonstrate that uSkin can be easily adapted, this time the sensor will be installed on a humanoid robot, iCub, and perform an object shape exploration task. The new soft skin consists of two different materials, structured silicone and fabric. A different material and structure will result in different characteristics of the sensor. Therefore, different calibration approaches need to be evaluated and a characterization of the sensor needs to be conducted again.

Thus, the main contributions of this work are that 1) we propose and evaluate the new structure of the skin, 2) improve the sensor's sampling frequency and reduce the size of the readout electronics with minimized wiring, 3) test the sensor's durability to overloading, and 4) use the sensor for shape exploration with iCub.

The rest of this paper is organized as follows. In Section II we provide a review of related soft skin sensors. Section III describes the new sensor structure, the manufacturing process, and the integration into iCub's hand. Section IV presents the experimental procedure that was used to evaluate the sensor and shows the results. Section V shows the object exploration with iCub. Section VI draws conclusions and presents future work.

II. RELATED WORKS

Many tactile sensors have been developed but only a few of them can be used to cover various robot parts and can measure multi-axis force [8] [9]. OptoForce[1] sells a small 3-axis sensor but the size is still 10 mm wide and 8 mm high. Touchence[2] sells a thin, small-sized 3-axis microelectromechanical systems (MEMS) sensor which uses piezoelectric elements. This sensor is rigid and requires additional electronics, which are bigger than the sensor itself. Implementing distributed 3-axis force sensing using these sensors seems difficult. A robotic fingertip that is multi-modal and can measure distributed force is available from SynTouch[3]. However, this sensor can only measure one axis force for each taxel and cannot easily be adapted to cover various robot parts.

The robot in [10] is covered with tri-axial skin sensors based on strain gauges. However, because of the sensor size, using them for distributed sensing in robot hands may not be feasible. Some robots have distributed skin sensors [11] [12] [13] but each load cell can only measure normal force.

Soft skin sensors with capacitive sensing technology have been introduced in [11] [12] [14]. The Sugano lab has developed a human-symbiotic robot, Twendy-One, covered with soft skin sensors [11]. For each hand, there are 133 of 4x4 mm sensing elements on its fingertips and 108 of 7.5 x 7.5 mm sensing elements on its phalanges. However, the sensor can only measure normal force and requires additional electronics which consume a lot of space and increase the weight. In

[12], the whole robot is almost fully covered with capacitive skin sensors. Moreover, the large-scale tactile data can be handled with a minimum number of wires thanks to using a small sized AD7147 capacitance to digital converter chip. The output is already digital and can be connected directly to the microcontroller (called "MTB") through I2C connection. However, the sensor can only measure normal force as well. A 3-axis capacitive-based skin sensor has been developed using the same chip by implementing tilted sensing pads to measure shear forces [14]. However, in a 14 x 14 x 7 mm area, only 1 force vector can be measured. Therefore, the spatial density for a 3-axis distributed force sensing application is limited and smaller sized sensors would also make it is easier to adapt the sensor for various shapes.

To solve this problem, we implemented a Hall-effect based force sensing approach. The idea of using Hall-effect based skin sensing was introduced in [15] and [16]. These works only presented preliminary prototypes without detailed characterization. Recently, the MLX90393 chip from Melexis, a small sized 3-axis Hall-effect sensor, became available. This sensor is 3x3x1 mm big, has digital output and can be connected directly to a microcontroller through I2C connection. As a result, we successfully developed a first skin sensor prototype including its characterization in [5]. Later, we implemented distributed sensing using this chip to cover robot fingers and phalanges [6] [7]. As a result, 3-axis force sensing with a spatial density of 4.7 mm could be achieved. However, even though the sensor provides digital output, rather bulky readout electronics were used. Moreover, the magnets were embedded in bulk silicone, causing severe crosstalk between the 3 measurement axis.

The significance of our work compared to previous works (especially Hall-effect based) is that [17] [18] show that the sensor can be integrated into a robot hand but only measure 1-axis; [19] proposes a 3D sensor, but the sensors were not used for distributed sensing; [20] [21] has been successfully applied to real robotic scenarios, but the design they proposed (with a rubber dome and four Hall effect sensors) imposed constraints on the minimum size of each sensor. [17] [18] implemented an air gap for increased sensitivity for 1-axis sensing and in [22] for 3-axis sensing. The current work also uses an air gap, however in [17] [18] [22] only one sensor for one finger phalange was implemented, and a different structure is required for dense distributed skin sensing; moreover, the importance for reducing the crosstalk for 3-axis sensing was not investigated.

In summary, a practical distributed soft skin sensor system that can cover various parts of the robot hand, measure force in 3-axis, with a subcentimeter spatial density, digital output and small readout electronics at the same time does not exist yet. The system presented in this paper has all these features and is moreover low cost in terms of the required materials and labor effort. Compared to our previous work we show the implementation of the new skin structure for reduced 3-axis crosstalk and small sized readout electronics.
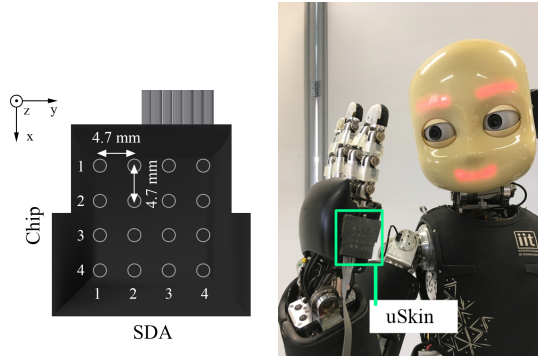
---

[1] http://optoforce.com/

[2] http://www.touchence.jp/

[3] https://www.syntouchinc.com/

Fig. 1. SDA and chip placement (left). Humanoid robot, iCub, and uSkin mounted on its hand (right).

Fig. 2. Design of uSkin for iCub.

TABLE I
AR-G1L SPECIFICATIONS

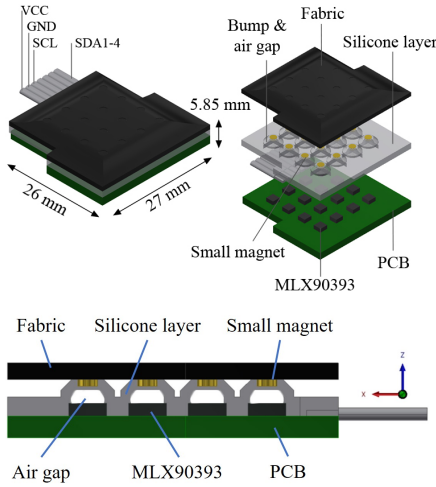| Details	Unit	Test	AR-G1L
Shore hardness (A)	-	JIS K6253	35
Elongation ratio at break	%	JIS K6251	160
Tensile strength	MPa	JIS K6251	0.5-0.8
Tearing strength	kg/cm	JIS K6252	3.1
Density	g/cm^3	JIS K6268	1.03
Water absorption	%	JIS K7209	less than 0.4

III. SENSOR DESCRIPTION

In this section, after a short description of the general working principle of the sensor, we introduce uSkin's improvements compared to the previous generation, including the new sensor's structure and readout electronics.

A. Sensing Principle and Improved Skin Structure

The sensing principle is described as follows. The permanent magnet displacements in x, y, and z-axis are measured based on the magnetic field changes detected by the MLX90393 chip. These magnetic field changes are then converted into force according to a calibration process that will be explained in the next section. The uSkin used in this paper has a size of 26x27x6.05 mm and has a spatial density of 4.7 mm between each 3-axis load cell, see Fig. 2. We used the same PCB with 16 MLX90393 chips that was previously introduced in [6]. The previous skin structure had 16 magnets that were embedded inside bulk silicone rubber. Bulk silicone (which is deformable, but incompressible) potentially causes the magnets to displace sideways when only normal force is applied, and indeed we observed crosstalk between the 3-axis measurements [6]. To minimize this crosstalk effect, we improved the skin structure with bumps and air gaps as can

be seen in Fig. 2. This deformable bump-like structure can also act like a spring. The air gap between the chip and the silicone is 1.7 mm high. In total the sensor is 6.05 mm thick (1.7 mm thick PCB, 2.85 mm silicone including magnets and chip, 1.5 mm fabric).

B. Soft Skin Manufacturing Process & Mounting on iCub

The soft skin introduced in this paper consists of two layers as in Fig. 2. The layer above the PCB is made from silicone and the top layer is a fabric. The bottom layer was printed using a 3D printer that can print a silicone rubber material (Agilista 2000 from Keyence). The material was AR-G1L (specifications according to datasheet are listed in Table I). It is harder than Ecoflex 50 from Smooth-On, which we have used in past work. There are two reasons why we selected AR-G1L. First, initially we tried to mold the silicone structure with Ecoflex 50, but the skin was too soft and the 16 permanent magnets were attracted to each other. AR-G1L is stiff enough to maintain the shape of the structure when not loaded while it is still deformable and provides a reasonable force measurement range. Second, a complex structure can be 3D printed rapidly and effortlessly compared to molding thin silicone.

The silicone layer consists of a bump-like structure with 16 small holes to place the permanent magnets inside. We used a silicone glue (Sil-Poxy from Smooth-On; working time 5 minutes, cure time 12 minutes at 23°C) to fix the magnets and prevent them from flipping. After the silicone glue completely cured, we covered it with a top layer (Neoprene from RS Pro, RS stock no. 733-6753, with 1.5 mm thickness). The fabric was glued on the top of the silicone using Power Flex, a flexible super glue from Loctite (15-30 s fixture time). The skin layer was then fixed on the PCB using the same super glue. Afterwards, the PCB module covered with the skin (uSkin module) was mounted to iCub's hand using a strong double-sided sticky tape (VHB from 3M, white, about 1mm thick) as shown in Fig. 1 (right).

C. Improved Readout Electronics

In our previous work, we used bulky electronics (one Arduino Due with one TCA9548A, an I2C multiplexer from Adafruit) to read 3 axis x 16 chips measurements from one module. One Arduino Due has only two I2C data (SDA) buses. Meanwhile, one uSkin module with 16 chips (with a 2
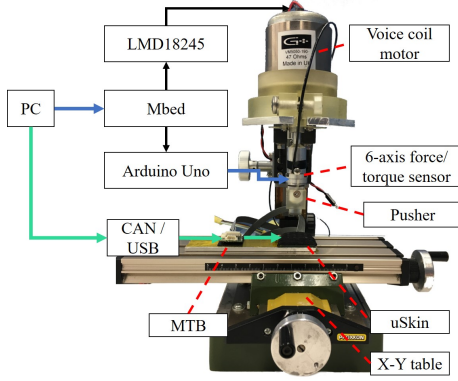
Fig. 3. Test setup

bit variable address) requires four buses. For this reason, the multiplexer was necessary to acquire data from four buses. As a result, the sampling frequency was limited to only up to 30 Hz. This time we improved the electronics by using a MTB3, a small microcontroller developed by IIT (Istituto Italiano di Tecnologia) for their humanoid robot iCub [23] [12]. The MTB3 is about 26x18x6 mm big, has 4 SDAs for I2C communication, and can be daisy-chained through CAN (Controlled Area Network) bus. Therefore, one MTB3 is enough to handle all 16 MLX90393 chips' measurements with a higher sampling rate. A single MLX90393 chip can provide 3-axis magnetic field and one temperature measurement with a sampling rate of up to around 500 Hz, according to the configuration of the built-in digital filter. However, a higher frequency will have more noise as a trade off. Therefore, for the current paper we configured our sensor with a digital filter setting allowing a maximum frequency of about 125 Hz; the MTB3 was set to collect measurements with 100 Hz, which could easily be increased in future work. Overall, in addition to the improved sampling frequency, the readout electronics are more compact than in our previous work and the required number of wires is minimized; seven wires, i.e. 1 VCC (power, which is 3.3V), 1 GND (ground), 4 SDAs, and 1 SCL (clock) for the communication between the uSkin module and the MTB3, and 4 wires (1 VCC, 1 GND, 1 Tx, and 1 Rx) for the communication between 2 microcontrollers or the serial communication of the MTB3 with the CAN-USB or CAN-ethernet converter, which is connected to the PC.

IV. SENSOR CHARACTERIZATION

In this section, uSkin's characteristics such as its durability, calibration model and SNR model will be provided.

A. Experimental Setup

Fig. 3 shows the complete test setup used in this paper. The reference sensor is a Nano 1.5/1.5, a 6-axis force/torque (F/T) sensor from BL Autotech. A cylindrical 3D printed plastic pusher with 10 mm diameter was attached to this sensor. Shear forces can be applied after an initial contact by displacing

the skin sensor with the x-y table. uSkin was mounted to the x-y table using a thin double sided sticky tape from 3M. To apply various perpendicular load forces, we use a voice coil motor (VM5050-190 from Geeplus). In previous work we used an Arduino Due to produce analog ouput (DAC) for the current control (which is subsequently amplified), but the Arduino Due's minimum output is not zero, and therefore we could not produce forces of less than 1 N with the voice coil motor. Therefore, in the current test setup we use an mbed LPC1786 microcontroller; the resolution is only 10 bit, but using it we can produce a step force of about 0.25 N starting from 0 N. The 6-axis F/T and all MLX90393 measurements are collected with 100 Hz. 50 samples before and after each force change were removed. An offset for each sensor sensor axis is calculated from the average of the first second of measurements. No further filters (except the one in the chip) were used.

B. Sensor Response before Calibration

Two kinds of skin structure were compared: bulk silicone (as in our previous work [6] [7]) and the new structure with bumps and air gaps. In Fig. 4 (top) shows the response with bulk silicone. Even though only z-axis force was applied, the skin sensor also measures x-axis displacement. This happened most likely because the permanent magnet was displaced sideways as a result of the incompressibility of the silicone material. In Fig. 4 (bottom), the response of uSkin with bumps and air gaps can be seen. The graph shows less response in x and y-axis. We calculated the crosstalk between the 3 axis measurements as $mean(abs(S_x/S_z) + abs(S_y/S_z))$ (mean of all time steps when being pushed with z-axis force; data taken from Fig. 4 and from [7] for the curved sensor, respectively). The results are shown in Table III. The crosstalk between the 3-axis measurements in % went from around 40% to around 4%, and is therefore about 10 times less.

C. Durability

In this experiment, we tested uSkin's durability by applying a high load, see Fig. 5. In the first 5 s, no load was applied. Subsequently, uSkin was loaded with around 50 N of normal force (about 637 kPa) for 10 s. As the distance of the permanent magnet got too close to the chip, the uSkin measurement had an overflow. Finally, uSkin was unloaded and all axis readings gradually return towards zero. Subsequently, after receiving high pressure, uSkin was still working normally.

D. Calibration

This section describes how to calculate 3-axis force out of uSkin's raw measurements.

1) Training set preparation: Five datasets consisting of input (uSkin's raw measurements) and target (the reference sensor's 3-axis force measurements) were provided to find the calibration parameters. In particular, normal force and shear forces in +x, -x, +y and -y direction were applied on top of chip 3, SDA 3. The five datasets were combined, i.e. all data was used to find the calibration parameters for all axes. Only
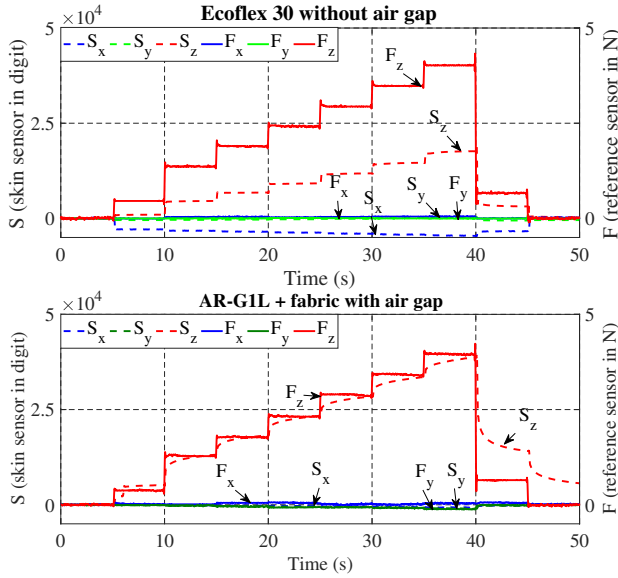
Fig. 4. Sensor response when subject to stepwise z-axis force with bulk silicone (top) and new structure (bottom).
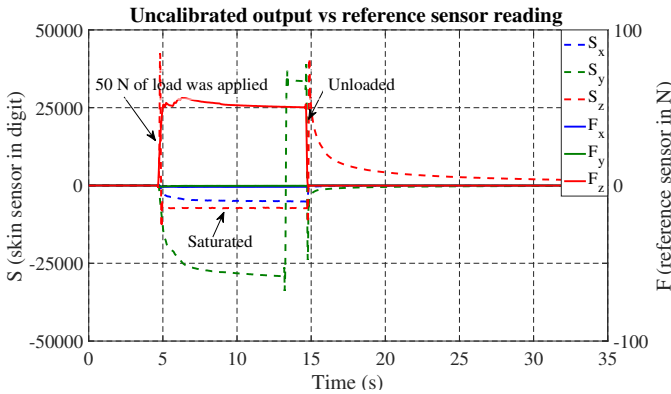

Fig. 5. Overloading test.

TABLE II
R-SQUARED COMPARISON VALUE.

Calibration method	R-squared value		
	z-axis	x-axis	y-axis
Quadratic + Huber	0.1091	0.7158	0.4129
Linear + Huber	0.8532	0.9179	0.9028
FNN (1 HL with 5 units)	0.8420	0.9100	0.9105

and the Neural Network Toolbox in MATLAB, respectively. In our previous works, we found that the best method for calibrating the sensor was linear regression with a quadratic model (and the robust Huber option). The material used was silicone rubber from Ecoflex with shore hardness 00-30 and 00-50 without an air gap. Since we use a new structure and different materials in the current paper, a comparison between each fitting method should be conducted again. We selected three different methods, linear regressions with and without quadratic model (both with Huber robust option) and a feed-forward neural network (FNN) with 1 hidden layer.

To find the calibration parameters with the FNN method, we divided the data into 70 % for training and 30 % for validation. The FNN parameter learning was performed with 8 different hidden layer sizes. 1, 2, 3, 4, 5, 10, 20, and 30 neurons formed the hidden layer. We used three neural networks for calibrating a single chip, one for each axis. The inputs were the raw x, y, z measurements of the chip; the target output was either the x, y, or z-axis of the F/T sensor. The BFGS quasi-Newton backpropagation algorithm was selected. The iteration was limited to 1000 steps. The R-squared value (calculated from data not included for training) of the x-axis calibration starts to slightly decrease with more than 5 hidden units. Also the other axis are barely improving with more than 5 hidden units.

The calibration performance results for all methods can be seen in Table II. New data (not used for calculating the calibration parameters) collected for 3 axis in the same fashion as the training set was used for this table. Overall, the simple linear model already provided nearly the best results compared to the other methods. This is congruent with other results obtained with our sensor. In another preliminary experiment we used foam as the deformable material, and again the linear model provided nearly the best results in all cases. On the other hand, in our previous work with bulk silicone the quadratic model outperformed the linear model [6] [7]. We extrapolate as a general trend that a linear model is sufficient for a compressible structure or material, but a quadratic model performs better in the incompressible case. However, it should also be mentioned that the R-squared values for calibrating the z-axis with the linear model for the current sensor (0.8532) are comparable or even slightly lower than in our previous works (0.8634 for the flat module with bulk silicone and a linear model, and 0.8938 for the curved fingertip). We assume that the increased hysteresis in the current sensor makes the force calculation less precise in general. Finally, we selected the linear model for the calibration of the current version of
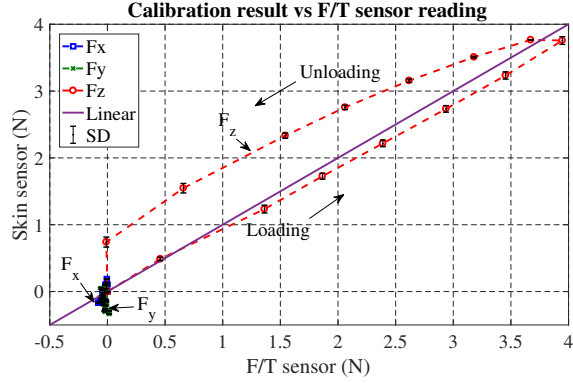
one chip was investigated as the data collection for the shear force is currently done manually and is very time consuming; a rough analysis showed that some taxels could be about twice as sensitive as others in the z-axis. In future work we will use an motorized x-y stage to perform a comparative analyses between the taxels and to provide automated calibration; also the sensor production (in particular gluing the textile) could be automated to reduce the differences between taxels.

For the normal force, the force was increased in steps of 0.5 N every 5 + 10 seconds (5 s pushing, 10 s no contact of pusher with skin), and 5 different forces were applied in total. For the +x shear force, first normal force of 3.5 N was applied, and then every 4 s the skin sensor was displaced by 0.2 mm by manually turning the knob of the x-y table; 7 steps of shear force were applied. The same procedure as for the +x shear force was used for the other three shear forces as well.

2) Calibration methods: To find the calibration parameters, different methods such as curve fitting or a neural network can be used. We employ the Statistics & Machine Learning toolbox
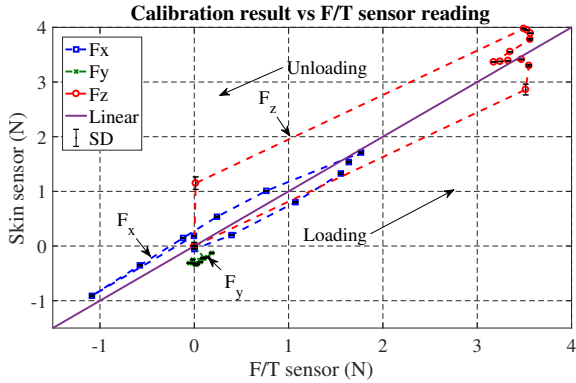
Fig. 6. Calibrated sensor response when normal force is applied.

Fig. 7. Calibrated sensor response when shear force is applied.

uSkin. (1) shows the calibration model.

$$S_{j,c} = aS_x + bS_y + cS_z \qquad (1)$$

Here, $S_{j,c}$ is the calibrated sensor output of axis j (x, y, or z). S_x, S_y, and S_z are pre-calibrated skin sensor module outputs in digits. a, b, and c are the calibration parameters calculated in MATLAB using the Statistics & Machine Learning Toolbox.

3) Calibration Result: Fig. 6 shows the calibrated z-axis measurement of uSkin. Fig 7 and 8 show the response for x-axis and y-axis, respectively. For all three figures the force in the respective axis was stepwise increased and then decreased (unlike the training set for the calibration parameters, in which the force was only stepwise increasing). Also, while there were 10 s breaks between the steps in the data with stepwise increasing z-axis force used for calibration, in the data for Fig. 6 there were no breaks between the steps.

E. Hysteresis

A soft material can introduce hysteresis to the system, and the output of the sensor during the unloading cycle can be different than during the loading cycle. This can happen because the soft material requires some time to completely return to its initial state. Furthermore, in Fig 7 and 8 the z-axis force measurement of the skin sensor increases by about 1 N, even though the actual force is rather stable or even
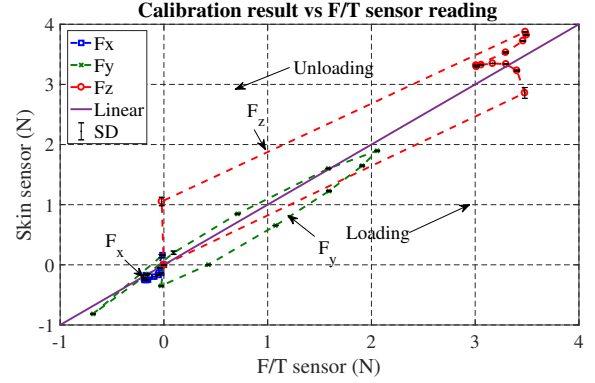

Fig. 8. Calibrated sensor response when shear force is applied.

decreases (variations in the applied force are due to limitations in the force control of the voice coil motor, i.e. friction). The hysteresis value can be calculated using (2).

$$Hysteresis \ \% = \left| \frac{(F_{mu} - F_{ml})}{(F_{max} - F_{min})} \right| \times 100\% \qquad (2)$$

F_{min} was the minimum and F_{max} the maximum measured average force by the reference sensor. F_{ml} and F_{mu} are the calibrated skin force values (linear interpolation of the nearest neighbors) of the loading and unloading cycles, respectively. These two values were taken at the midpoint of the cycle (X_m) as calculated using (3).

$$X_m = \left(\frac{F_{max} - F_{min}}{2} \right) + F_{min} \qquad (3)$$

Using the loading and unloading cycle in Fig. 6, 7 and 8, we found that the hysteresis was about 20.5 % for the z-axis, 12.2 % for the x-axis, and 16.8 % for the y-axis.

F. Signal to noise ratio

The SNR (signal to noise ratio) value in decibel (dB) of each taxel for different loads can be calculated as

$$SNR_{dB} = 20 \log_{10} \left(\frac{|\mu_U - \mu_p|}{\sigma_u} \right) dB \qquad (4)$$

where μ_U and σ_u are the average and standard deviation value of the calibrated uSkin measurements when there was no force applied. μ_p is the average value of the calibrated uSkin measurement when the skin was pushed.

The SNR results of one sensor for different pressures are presented in Table III, together with an overview of other relevant results. Table III also shows a comparison to the results with bulk silicone for flat [6] and curved modules [7]; the SNR values for those sensors were calculated from new data taken with the new measurement electronics presented in the current paper, at the same measurement frequency, and with the same 10 mm diameter cylindrical pusher. The SNR values are overall similar and lie within the normal variation that can be observed in our experiments between different loadcells (the noise as well as sensitivity varies between sensors). All results will be further discussed in Section VI.

TABLE III
COMPARISON TABLE

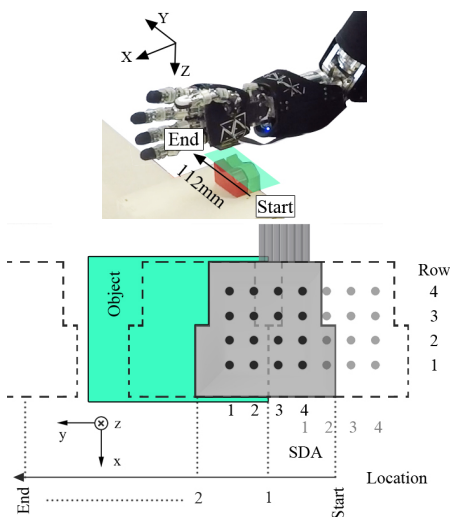|	flat	curved	new structure
Pressure (kPa)		SNR (dB)	
4.5	48.04	47.62	39.06
7.6	53.35	51.51	47.44
9.4	55.49	52.61	50.67
12.6	58.89	53.29	54.56
Hysteresis z-axis (%)	5.29	10	20.5
Range (N)	14	6	14
Thickness (mm)	4	4	5.85
Crosstalk during z-axis pushing (%)	41.48	38.48	3.86

Fig. 9. Experimental setup for shape exploration task (top). Illustration of exploration procedure (bottom).

V. IMPLEMENTATION ON ICUB

uSkin with the new structure was mounted on iCub and used for object exploration. iCub was pushing against objects in different locations with a certain force within the optimal range of forces for the skin sensor (controlled as compliance). The compliance was set only on the three shoulder joints (pitch, roll, yaw) and on the elbow joint, while the other joints were position controlled. Four objects with different shapes (but same length and width of 5 x 3 cm when seen from above) were used. We named them arc, flat, wave, and saw. iCub pushed the sensor 8 times against each object as illustrated in Fig. 9 (bottom). The overlap was 50 % of the module size. As a result, all chips on SDA 4 will always be on top of SDA 1 of the previous step. For that reason, we remove all data from SDA 1.

The exploration results can be seen in Fig. 10. The data (raw sensor measurements) from all 8 exploration steps is shown in the same graph, and the graphs only show the z-axis measurements for easier comprehensibility. The raw shear measurements provide little information to the naked eye for the current task, but are overall as expected, i.e. the

measurement vector is somewhat perpendicular to the object surface. From Fig. 10 it can be seen that the measurements from row no. 3 and 4 were the most responsive. Furthermore, especially when looking at the flat object, it can be seen that SDA 2 and 3 responded stronger than SDA 1. Those differences could be due to two reasons. First, the iCub hand was not perfectly perpendicular when it pushed the object. Second, we show uncalibrated sensor responses, and some taxels are more sensitive than others. Moreover, the y-axis displacement shown in the plots is only indicative, as iCub has compliance in its arms, which would explain some of the differences in the locations of the sensor response and the corresponding object features such as corners. The sensor module is also T-shaped, and sometimes the edge of the sensor module was in contact with the object, and none of the sensors responded, which is particularly evident when looking at the response to arc.

Despite all these factors, the first 3 objects provided very distinctive results. The results from wave and saw look similar, which is understandable, as they have a similar shape. However, the saw shape has two peaks in the 30 - 50 mm location while wave only has one. Possibly the pressure produced from the sharp edge was higher and can be detected.

VI. CONCLUSIONS AND FUTURE WORK

This paper presented a new structure for the soft skin of uSkin. Table III shows the most important characteristics and compares them to the previous versions of uSkin. Most importantly, the crosstalk between the 3-axis (due to the incompressibility of silicone material) was reduced (from around 40% to about 4%). Even without a time consuming calibration of the sensor, the 3-axis components are therefore more independent. The SNR was comparable and lies within the normal variation between different loadcells that we observed in our experiments. The range was also similar to the previous flat version. The sensor was thicker, but this does not constitute an inherent weakness of the current sensor, as it was partially due to the rather thick Neoprene (1.5 mm thickness) and partially due to the PCB (we used a 1.7 mm thick PCB, which is otherwise identical to the 0.5 mm thick PCB in [6], to increase the stability, as the iCub hand does not provide a flat support for the sensors). Therefore, the sensor thickness can be easily reduced in future work. The hysteresis was increased. This is due to the material, which has a visibly high hysteresis also when used in bulk form. Future work could use the new structure with a material with less hysteresis. However, currently few soft materials can be 3D printed, and 3D printing facilitates the prototype production compared to molding. Furthermore, we could show that despite using structured silicone, the sensor was robust to overloading with 50 N (about 637 kPa). Overall, we proved that it is easy to configure uSkin for different requirements. Using a textile as the top layer can be beneficial depending on the application. Aside from the new skin structure, we also implemented iCub's MTB3 microcontrollers for uSkin to increase the sampling frequency, reduce the size of the readout electronics, and to minimize the required wires. Finally, we
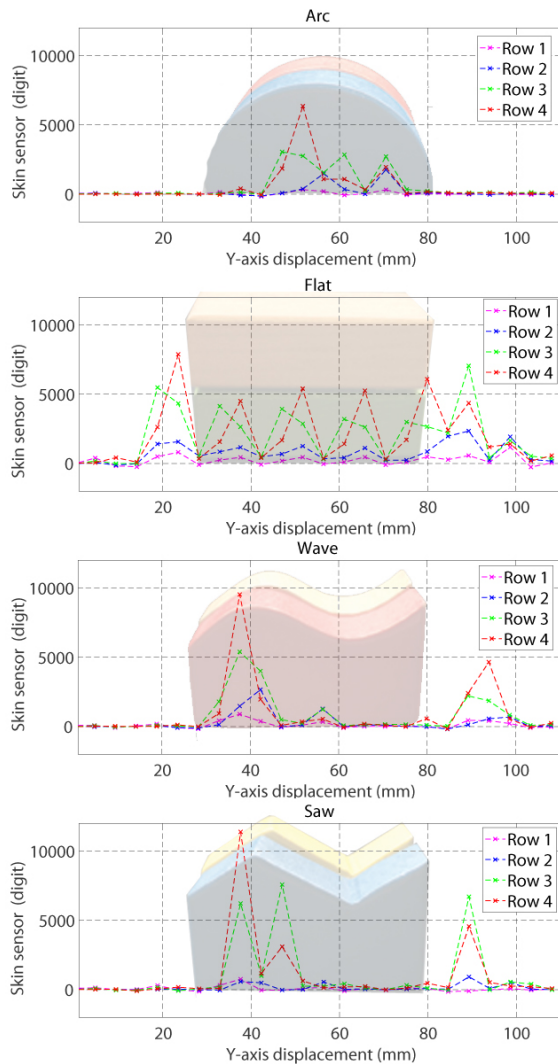
Fig. 10. Shape exploration response (uncalibrated z-axis measurements at different positions: 0 mm - SDA 4, 4.7 mm - SDA 3, 9.4 mm - SDA 2, 14.1 mm - SDA 4 of second exploration step, and so on.

did first tests with uSkin mounted on an iCub, and showed that the sensors can be used to differentiate object shapes. In future work we plan to use a motorized x-y stage to automatically calibrate all sensors and perform a comparative analysis between taxels. Also the production process (such as gluing the fabric) could be automated to reduce the difference between taxels.

References

[1] Z. Kappassov, J.-A. Corrales, and V. Perdereau, "Tactile sensing in dexterous robot hands–Review," *Robotics and Autonomous Systems*, vol. 74, pp. 195–220, 2015.
[2] M. Cutkosky, J. Jourdain, and P. Wright, "Skin materials for robotic fingers," in *ICRA*, vol. 4. IEEE, 1987, pp. 1649–1654.
[3] T. Hoshi and H. Shinoda, "Robot skin based on touch-area-sensitive tactile element," in *ICRA*, 2006, pp. 3463–3468.
[4] V. Duchaine, N. Lauzier, M. Baril, M. A. Lacasse, and C. Gosselin, "A flexible robot skin for safe physical human robot interaction," in *ICRA*, 2009, pp. 3676–3681.
[5] T. P. Tomo, S. Somlor, A. Schmitz, L. Jamone, W. Huang, H. Kristanto, and S. Sugano, "Design and characterization of a three-axis hall effect-based soft skin sensor," *Sensors*, vol. 16, no. 4, p. 491, 2016.
[6] T. P. Tomo, W. K. Wong, A. Schmitz, H. Kristanto, A. Sarazin, L. Jamone, S. Somlor, and S. Sugano, "A modular, distributed, soft, 3-axis sensor system for robot hands," in *2016 IEEE-RAS Humanoids*. IEEE, 2016.
[7] T. P. Tomo, A. Schmitz, W. K. Wong, H. Kristanto, S. Somlor, J. Hwang, L. Jamone, and S. Sugano, "Covering a robot fingertip with uSkin: A soft electronic skin with distributed 3-axis force sensitive elements for robot hands," in *2017 IEEE/RSJ IROS*. IEEE, 2017.
[8] R. S. Dahiya, P. Mittendorfer, M. Valle, G. Cheng, and V. J. Lumelsky, "Directions toward effective utilization of tactile skin: A review," *IEEE Sensors Journal*, vol. 13, no. 11, pp. 4121–4138, 2013.
[9] R. S. Dahiya, G. Metta, M. Valle, and G. Sandini, "Tactile sensing–from humans to humanoids," *IEEE Transactions on Robotics*, vol. 26, no. 1, pp. 1–20, 2010.
[10] T. Yoshikai, M. Hayashi, Y. Ishizaka, H. Fukushima, A. Kadowaki, T. Sagisaka, K. Kobayashi, I. Kumagai, and M. Inaba, "Development of robots with soft sensor flesh for achieving close interaction behavior," *Advances in Artificial Intelligence*, vol. 2012, p. 8, 2012.
[11] H. Iwata and S. Sugano, "Design of human symbiotic robot TWENDY-ONE," in *ICRA*. IEEE, 2009, pp. 580–586.
[12] A. Schmitz, P. Maiolino, M. Maggiali, L. Natale, G. Cannata, and G. Metta, "Methods and technologies for the implementation of large-scale robot tactile sensors," *IEEE Transactions on Robotics*, vol. 27, no. 3, pp. 389–400, 2011.
[13] W. Fukui, F. Kobayashi, F. Kojima, H. Nakamoto, N. Imamura, T. Maeda, and H. Shirasawa, "High-speed tactile sensing for array-type tactile sensor and object manipulation based on tactile information," *Journal of Robotics*, vol. 2011, 2011.
[14] S. Somlor, R. S. Hartanto, A. Schmitz, and S. Sugano, "A novel tri-axial capacitive-type skin sensor," *Advanced Robotics*, vol. 29, no. 21, pp. 1375–1391, 2015.
[15] J. J. Clark, "A magnetic field based compliance matching sensor for high resolution, high compliance tactile sensing," in *ICRA*. IEEE, 1988, pp. 772–777.
[16] W. C. Nowlin, "Experimental results on Bayesian algorithms for interpreting compliant tactile sensing data," in *ICRA*. IEEE, 1991, pp. 378–383.
[17] L. Jamone, G. Metta, F. Nori, and G. Sandini, "James: A humanoid robot acting over an unstructured world," in *6th IEEE-RAS International Conference on Humanoid Robots*. IEEE, 2006, pp. 143–150.
[18] L. Jamone, L. Natale, G. Metta, and G. Sandini, "Highly sensitive soft tactile sensors for an anthropomorphic robotic hand," *IEEE sensors Journal*, vol. 15, no. 8, pp. 4226–4233, 2015.
[19] C. Ledermann, S. Wirges, D. Oertel, M. Mende, and H. Woern, "Tactile sensor on a magnetic basis using novel 3D Hall sensor-First prototypes and results," in *17th International Conference on Intelligent Engineering Systems*. IEEE, 2013, pp. 55–60.
[20] S. Youssefian, N. Rahbar, and E. Torres-Jara, "Contact behavior of soft spherical tactile sensors," *IEEE sensors Journal*, vol. 14, no. 5, pp. 1435–1442, 2014.
[21] E. Torres-Jara, I. Vasilescu, and R. Coral, "A soft touch: Compliant tactile sensors for sensitive manipulation," 2006, [Online; accessed 6-February-2018].
[22] T. Paulino, P. Ribeiro, M. Neto, S. Cardoso, A. Schmitz, J. Santos-Victor, A. Bernardino, and L. Jamone, "Low-cost 3-axis soft tactile sensors for the human-friendly robot Vizzy," in *ICRA*, 2017.
[23] G. Cannata, M. Maggiali, G. Metta, and G. Sandini, "An embedded artificial skin for humanoid robots," in *IEEE International Conference on Multisensor Fusion and Integration for Intelligent Systems*. IEEE, 2008, pp. 434–438.